

APPLICATIONS OF SLIDING MODE CONTROL TO BENCHMARK PROBLEMS

J. C. WU^{1,*†}, J. N. YANG^{2,‡} AND A. K. AGRAWAL^{3,§}

¹ *Department of Civil Engineering, Tamkang University, Taipei, Taiwan, Republic of China*

² *Department of Civil and Environmental Engineering, University of California, Irvine, CA 92697, U.S.A.*

³ *Department of Civil Engineering, The City College of the City University of New York, NY 10031, U.S.A.*

SUMMARY

In this paper, both the methods of continuous sliding mode control (CSMC) and continuous sliding mode control with compensators (CSMC&C) have been applied to two benchmark structures, namely, a building model equipped with an active mass driver system, and a building model equipped with an active tendon system. The CSMC&C strategy is a modification of CSMC to facilitate the design of static output feedback controllers and to provide a systematic tuning of the control effort. Due to the structural identification scheme used in the benchmark problems, in which the state variables are fictitious, one cannot take the full advantages of static output feedback controllers. As a result, an observer is used in CSMC, whereas a low-pass filter is incorporated for each measurement in CSMC&C. The purpose of using low-pass filters in CSMC&C is to transform the benchmark problems into strictly proper systems. The main advantage of the CSMC&C method is that the on-line computational effort is reduced since the dimension of filters and compensator is much smaller than that of an observer. Simulation results based on the CSMC and CSMC&C methods are presented and compared with that of the LQG method. Robustness of stability and noise rejection for each controller design are also illustrated by examining the loop transfer function. Simulation results for the benchmark problems indicate that the control performances for LQG, CSMC and CSMC&C are quite comparable. © 1998 John Wiley & Sons, Ltd.

KEY WORDS: sliding mode control; compensator; benchmark problem; active driver system; active tendon system; low-pass filter

1. INTRODUCTION

The theory of sliding mode control (SMC) or variable structure system (VSS) was developed for robust control of uncertain non-linear systems.^{1,2} Its main idea is to design a controller to drive the response trajectory into the sliding surface, in which the motion of the system is stable. Applications of continuous sliding mode control (CSMC) that does not have chattering effect to the following seismic-excited structures have been studied: (i) linear and nonlinear or hysteretic buildings,^{3–6} (ii) sliding-isolated buildings⁷ and (iii) parametric control, such as the use of active variable dampers (AVD) on bridges⁸ and active variable stiffness (AVS) systems.⁹ In addition to full-state feedback controllers, static output feedback controllers using only a limited number of sensors installed at strategic locations were also presented in the studies above. Shaking table experimental verifications of the CSMC methods for linear and sliding-isolated building models have been conducted.^{7,10} Based on the simulations and experimental results, it was demonstrated that the continuous sliding mode control methods are robust and their performances are quite remarkable.

* Correspondence to: J. C. Wu, Department of Civil Engineering, Tamkang University, Taipei, Taiwan, Republic of China

† Assistant Professor

‡ Professor

§ Assistant Professor

Recently, a technique for designing sliding mode controllers by introducing a fixed-order compensator has been presented,^{11–13} referred to as CSMC&C. The main advantages of using a fixed-order compensator in sliding mode control are as follows: (i) the static output feedback controller can be designed easily using the theory of linear quadratic regulator (LQR) static output feedback design, and (ii) the modulation of the response quantities and control efforts can be made in a systematic manner.

In this paper, both the methods of CSMC and CSMC&C are applied to two benchmark problems^{14,15} for the evaluation of their performances. For these two benchmark problems, the entire structure-control system is represented by the evaluation model from which the control performance is evaluated. The reduced-order model (or design model) with a smaller dimension is constructed for the controller design in order to reduce the time delay for on-line integration for dynamic output feedback controllers. Due to the identification scheme used in these two benchmark problems, the state variables are fictitious variables rather than the physical variables, such as displacements, velocities or accelerations. This excludes the applications and advantages of static output feedback controllers for CSMC and CSMC&C, since fictitious variables cannot be measured directly. Consequently, the dynamic output feedback controllers with on-line integration are used, and modifications have been made for CSMC and CSMC&C. For the CSMC method, an observer that is the modification of the Kalman–Bucy filter is implemented to estimate the state variables of the design model for computing the control command. For the CSMC&C method, a first-order low-pass filter is introduced for each feedback measurement to facilitate the dynamic output feedback design. Simulation results based on CSMC and CSMC&C are presented and their performances are compared with that of the LQG method. Since the control robustness for the stability and noise rejection for each controller design can be guaranteed by limiting the magnitude of the loop transfer function in the high-frequency range, the plots of loop transfer functions for three control strategies are also presented for comparison.

2. FORMULATION

For the benchmark problems, the interactions among the structure, control devices and earthquake were taken into account in the input–output relations, and the system dynamics is represented by the plant $\mathbf{P}(s)$ as shown schematically in Figure 1. The controlled plant has two inputs, i.e. the earthquake \ddot{x}_g and the actuator command u , and two outputs, i.e. the control output \mathbf{z} and measured output \mathbf{y} . The control output, consisting of response variables of the structure and control devices, is adjusted for the control objective. The measured output, consisting of direct measurements from the sensors, is used as the feedback quantities of control. The evaluation model given by Spencer *et al.*,^{14,15} is expressed as

$$\dot{\mathbf{x}} = \mathbf{A}\mathbf{x} + \mathbf{B}u + \mathbf{E}\ddot{x}_g \quad (1)$$

in which \mathbf{x} is the state vector consisting 28 state variables for the active driver system (or 20 state variables for the active tendon system), u is a scalar control command and \ddot{x}_g is the ground acceleration. The matrices \mathbf{A} , \mathbf{B} and \mathbf{E} are system matrix, control location matrix and excitation influence vector, respectively. The l -dimensional control output \mathbf{z} and m -dimensional measured output \mathbf{y} are given by

$$\mathbf{z} = \mathbf{C}_z\mathbf{x} + \mathbf{D}_zu + \mathbf{F}_z\ddot{x}_g \quad (2)$$

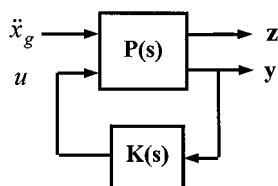


Figure 1. Control diagram for benchmark systems

and

$$\mathbf{y} = \mathbf{C}_y \mathbf{x} + \mathbf{D}_y u + \mathbf{F}_y \ddot{\mathbf{x}}_g + \mathbf{v} \quad (3)$$

respectively, in which \mathbf{C}_z , \mathbf{D}_z , \mathbf{F}_z , \mathbf{C}_y , \mathbf{D}_y and \mathbf{F}_y are matrices with appropriate dimensions and \mathbf{v} is the measurement noise vector. Hence, the plant $\mathbf{P}(s)$ can be partitioned as

$$\mathbf{P}(s) = \begin{bmatrix} \mathbf{P}_{z\ddot{x}_g} & \mathbf{P}_{zu} \\ \mathbf{P}_{y\ddot{x}_g} & \mathbf{P}_{yu} \end{bmatrix} \quad (4)$$

where

$$\begin{aligned} \mathbf{P}_{z\ddot{x}_g} &= \mathbf{C}_z(s\mathbf{I} - \mathbf{A})^{-1} \mathbf{E} + \mathbf{F}_z, & \mathbf{P}_{zu} &= \mathbf{C}_z(s\mathbf{I} - \mathbf{A})^{-1} \mathbf{B} + \mathbf{D}_z \\ \mathbf{P}_{y\ddot{x}_g} &= \mathbf{C}_y(s\mathbf{I} - \mathbf{A})^{-1} \mathbf{E} + \mathbf{F}_y, & \mathbf{P}_{yu} &= \mathbf{C}_y(s\mathbf{I} - \mathbf{A})^{-1} \mathbf{B} + \mathbf{D}_y \end{aligned} \quad (5)$$

In equations (2) and (3), the control output \mathbf{z} and measured output \mathbf{y} consist of the following physical quantities: (i) for the active mass driver system: $\mathbf{z} = [x_1, x_2, x_3, x_m, \dot{x}_1, \dot{x}_2, \dot{x}_3, \dot{x}_m, \ddot{x}_{a1}, \ddot{x}_{a2}, \ddot{x}_{a3}, \ddot{x}_{am}]'$ or their combinations, and $\mathbf{y} = [x_m, \ddot{x}_{a1}, \ddot{x}_{a2}, \ddot{x}_{a3}, \ddot{x}_{am}, \ddot{x}_g]'$, in which x_i is the displacement of i th floor relative to the ground, x_m is the displacement of the active mass driver relative to the 3rd floor, \ddot{x}_{ai} is the absolute acceleration of the i th floor, and \ddot{x}_{am} is the absolute acceleration of the mass driver, and (ii) for the active tendon system: $\mathbf{z} = [x_1, x_2, x_3, x_p, \dot{x}_1, \dot{x}_2, \dot{x}_3, \dot{x}_p, \ddot{x}_{a1}, \ddot{x}_{a2}, \ddot{x}_{a3}, f]'$ or their combinations, and $\mathbf{y} = [x_p, \ddot{x}_{a1}, \ddot{x}_{a2}, \ddot{x}_{a3}, f, \ddot{x}_g]'$, in which x_p and \dot{x}_p are the displacement and velocity of the actuator piston, and f is the tendon force. In the controller design, one has the freedom to choose appropriate control outputs and measured outputs from \mathbf{z} and \mathbf{y} given above, based on the control objective and the sensor installation. As a result, the matrices \mathbf{C}_z , \mathbf{D}_z , \mathbf{F}_z , \mathbf{C}_y , \mathbf{D}_y and \mathbf{F}_y should be modified appropriately to be consistent with \mathbf{z} and \mathbf{y} used.

With fictitious state variables, the controller can be designed such that the control command is computed on-line through dynamic output feedback that uses the measured output as feedback quantities. The transfer function of dynamic output feedback, $\mathbf{K}(s)$, is shown in Figure 1. To avoid serious time delay, the dimension of dynamic output feedback equations is restricted not to exceed 12 states. Therefore, a reduced-order design model with a dimension of r ($r \leq 12$) was constructed to provide a template for the controller design. In what follows, the vectors \mathbf{x}_r , \mathbf{y}_r , \mathbf{z}_r , \mathbf{F}_{zr} , \mathbf{F}_{yr} , \mathbf{E}_r and matrices \mathbf{A}_r , \mathbf{B}_r , \mathbf{C}_{zr} , \mathbf{D}_{zr} , \mathbf{C}_{yr} , \mathbf{C}_{yr} , \mathbf{D}_{yr} , are used to represent the corresponding vectors and matrices in the design model.

2.1. Continuous sliding model control (CSMC) using an observer

2.1.1. Design of sliding surface

The objective of CSMC is to design a controller to drive the state trajectory into a sliding surface (reaching condition) and maintain it there, whereas the sliding surface is designed to be stable. The sliding surface is expressed as $S = \mathbf{P}\mathbf{x}_r = 0$, where S is a scalar (since u is a scalar), and \mathbf{P} is a $(1 \times r)$ constant matrix called sliding surface matrix. To restrict the response trajectory to the sliding surface (i.e. $S = 0$ and $\dot{S} = 0$), and to stabilize the motion on the sliding surface, the matrix \mathbf{P} can be determined by minimizing the integral of a quadratic function

$$J = \int_0^\infty \mathbf{x}_r'(t) \mathbf{C}_r' \mathbf{Q} \mathbf{C}_r \mathbf{x}_r(t) dt \quad (6)$$

In Eq. (6), \mathbf{Q} is an appropriate $(l \times l)$ positive semi-definite weighting matrix.

2.1.2. Design of controller for reaching condition

The stable controller is designed such that a non-positive time derivative of a Lyapunov function $V = 0.5S'S$ is ensured at every time instant, i.e. $\dot{V} \leq 0$. The continuous sliding mode controller, in general, can

be expressed as^{3,5}

$$u = \mathbf{K}_b \mathbf{x}_r + K_f \ddot{x}_g \quad (7)$$

in which \mathbf{K}_b is the feedback gain and K_f is the feedforward gain given, respectively, by

$$\mathbf{K}_b = -(\mathbf{P}\mathbf{B}_r)^{-1} \mathbf{P}\mathbf{A}_r - \delta \mathbf{B}_r' \mathbf{P}' \mathbf{P} \quad (8)$$

and

$$K_f = -(\mathbf{P}\mathbf{B}_r)^{-1} \mathbf{P}\mathbf{E}_r \quad (9)$$

in which δ is the gain margin (scalar). Since the first term in equation (7) is the state feedback, a stable observer will be designed independently to estimate the state \mathbf{x}_r from the measured output \mathbf{y}_r based on the separation theorem.

2.1.3. Design of observer

First, we consider the case in which the feedforward compensation is ignored, i.e. $K_f = 0$. Assuming that the earthquake \ddot{x}_g and the measurement noise \mathbf{v} are uncorrelated Gaussian white noise processes, the well-known Kalman–Bucy filter can be modified as

$$\dot{\hat{\mathbf{x}}} = \mathbf{A}_r \hat{\mathbf{x}}_r + \mathbf{B}_r u + \mathbf{L}_0 (\mathbf{y}_r - \mathbf{C}_{yr} \hat{\mathbf{x}}_r - \mathbf{D}_{yr} u) \quad (10)$$

in which $\hat{\mathbf{x}}_r$ is the estimate of the state. The observer gain matrix \mathbf{L}_0 in equation (10) is obtained as

$$\mathbf{L}_0 = (\mathbf{P}_0 \mathbf{C}_{yr}' + \mathbf{S}_0) \mathbf{R}_0^{-1} \quad (11)$$

where \mathbf{P}_0 is the solution of the Riccati matrix equation

$$\mathbf{P}_0 \bar{\mathbf{A}} + \bar{\mathbf{A}}' \mathbf{P}_0 - \mathbf{P}_0 \mathbf{C}_{yr}' \mathbf{R}_0^{-1} \mathbf{C}_{yr} \mathbf{P}_0 + \mathbf{Q}_0 - \mathbf{S}_0 \mathbf{R}_0^{-1} \mathbf{S}_0' = 0 \quad (12)$$

in which

$$\bar{\mathbf{A}} = \mathbf{A}_r' - \mathbf{C}_{yr}' \mathbf{R}_0^{-1} \mathbf{S}_0' \quad (13)$$

In equations (11)–(13), \mathbf{Q}_0 , \mathbf{S}_0 and \mathbf{R}_0 are the partitions of the auto-power spectral density matrix of the vector $[\mathbf{E}_r' \ddot{x}_g, \mathbf{F}_{yr}' \ddot{x}_g + \mathbf{v}']'$, given by

$$\mathbf{Q} = \mathbf{E}_r S_{\ddot{x}_g \ddot{x}_g} \mathbf{E}_r', \quad \mathbf{S}_0 = \mathbf{E}_r S_{\ddot{x}_g \ddot{x}_g} \mathbf{F}_{yr}', \quad \mathbf{R}_0 = \mathbf{S}_{vv} + \mathbf{F}_{yr} S_{\ddot{x}_g \ddot{x}_g} \mathbf{F}_{yr}' \quad (14)$$

where $S_{\ddot{x}_g \ddot{x}_g}$ and \mathbf{S}_{vv} are the power spectral densities of \ddot{x}_g and \mathbf{v} , respectively.

With the feedback gain \mathbf{K}_b , the observer equation for on-line integration becomes

$$\dot{\hat{\mathbf{x}}}_r = (\mathbf{A}_r + \mathbf{B}_r \mathbf{K}_b - \mathbf{L}_0 \mathbf{C}_{yr} - \mathbf{L}_0 \mathbf{D}_{yr} \mathbf{K}_b) \hat{\mathbf{x}}_r + \mathbf{L}_0 \mathbf{y}_r \quad (15)$$

In addition to their individual stability, the observer gain \mathbf{L}_0 and controller gain \mathbf{K}_b should be designed to guarantee that $(\mathbf{A}_r + \mathbf{B}_r \mathbf{K}_b - \mathbf{L}_0 \mathbf{C}_{yr} - \mathbf{L}_0 \mathbf{D}_{yr} \mathbf{K}_b)$ is also stable. The control command in equation (7) at every sampling time instant is given by

$$u = \mathbf{K}_b \hat{\mathbf{x}}_r \quad (16)$$

and the $\mathbf{K}(s)$ matrix in the block diagram of Figure 1 can be expressed as

$$\mathbf{K}(s) = \mathbf{K}_b (s\mathbf{I} - \mathbf{A}_r - \mathbf{B}_r \mathbf{K}_b + \mathbf{L}_0 \mathbf{C}_{yr} + \mathbf{L}_0 \mathbf{D}_{yr} \mathbf{K}_b)^{-1} \mathbf{L}_0 \quad (17)$$

If the feedforward compensation K_f is included in the CSMC controller, the reduced-order design model can be expressed as

$$\dot{\mathbf{x}}_r = \mathbf{A}_r \mathbf{x}_r + \mathbf{B}_r u + \bar{\mathbf{E}}_r \ddot{x}_g \quad (18)$$

in which $\bar{\mathbf{E}}_r = \mathbf{E}_r + \mathbf{B}_r K_f$ and u involves only the feedback loop. Therefore, the design of the observer follows equations (10)–(15) except that the parameters \mathbf{Q}_0 and \mathbf{S}_0 are modified as

$$\mathbf{Q}_0 = \bar{\mathbf{E}}_r S_{\ddot{x}_g \ddot{x}_g} \bar{\mathbf{E}}_r', \quad \mathbf{S}_0 = \bar{\mathbf{E}}_r S_{\ddot{x}_g \ddot{x}_g} \mathbf{F}_{yr}' \quad (19)$$

Hence, the resulting control command at every sampling time instant is given by

$$u = \mathbf{K}_b \hat{\mathbf{x}}_r + \mathbf{K}_f \ddot{\mathbf{x}}_g \quad (20)$$

2.2. Continuous sliding mode control with compensator (CSMC&C)^{12,13,16}

For the design of CSMC&C controllers, instead of using an observer, a first-order filter is introduced for the measured output \mathbf{y}_r as follows:

$$\dot{\boldsymbol{\eta}} = \mathbf{A}_\eta \boldsymbol{\eta} + \mathbf{B}_\eta \mathbf{y}_r \quad (21)$$

where $\boldsymbol{\eta}$ represents the m -dimensional new output feedback vector, and \mathbf{A}_η and \mathbf{B}_η are filter coefficient matrices. Combining equation (21) and the state equation of the design model, one obtains the $(r + m)$ augmented design model

$$\dot{\tilde{\mathbf{x}}}_r = \tilde{\mathbf{A}}_r \tilde{\mathbf{x}}_r + \tilde{\mathbf{B}}_r u + \tilde{\mathbf{E}}_r \tilde{\mathbf{W}} \quad (22)$$

where

$$\tilde{\mathbf{x}}_r = \begin{pmatrix} \mathbf{x}_r \\ \boldsymbol{\eta} \end{pmatrix}, \quad \tilde{\mathbf{A}}_r = \begin{bmatrix} \mathbf{A}_r & 0 \\ \mathbf{B}_\eta \mathbf{C}_{yr} & \mathbf{A}_\eta \end{bmatrix}, \quad \tilde{\mathbf{B}}_r = \begin{pmatrix} \mathbf{B}_r \\ \mathbf{B}_\eta \mathbf{D}_{yr} \end{pmatrix}, \quad \tilde{\mathbf{E}}_r = \begin{pmatrix} \mathbf{E}_r & 0 \\ \mathbf{B}_\eta \mathbf{F}_{yr} & \mathbf{B}_\eta \end{pmatrix}, \quad \tilde{\mathbf{W}} = \begin{pmatrix} \ddot{\mathbf{x}}_g \\ \mathbf{v} \end{pmatrix} \quad (23)$$

The control output \mathbf{z}_r and the new measured output $\boldsymbol{\eta}$ for the augmented design model become

$$\mathbf{z}_r = \tilde{\mathbf{C}}_{zr} \tilde{\mathbf{x}}_r + \mathbf{D}_{zr} u + \mathbf{F}_{zr} \ddot{\mathbf{x}}_g \quad (24)$$

and

$$\boldsymbol{\eta} = \tilde{\mathbf{C}}_{yr} \mathbf{x}_r \quad (25)$$

where $\tilde{\mathbf{C}}_{zr} = [\mathbf{C}_{zr}, 0]$ and $\tilde{\mathbf{C}}_{yr} = [0, \mathbf{I}_m]$ with \mathbf{I}_m being an identity matrix of m dimension. Note that equation (25) has a strictly proper form. As observed from equations (22)–(25), the introduction of $\boldsymbol{\eta}$ provides the controller with the flexibility to make trade-off among the control output \mathbf{z}_r , the feedback output $\boldsymbol{\eta}$, and the control command u .

For the benchmark problems, the structural response is dominated by the lower-frequency component and the system uncertainty is more significant at high frequency. It is beneficial to weight more on the low frequency, and hence a low-pass filter is chosen such that the high-frequency component in \mathbf{y}_r is filtered out. For simplicity, the low-pass filter can be used independently for each measurement so that \mathbf{A}_η and \mathbf{B}_η are diagonal matrices with every diagonal element equal to a_i and b_i , respectively. One can further let $a_i = b_i$ such that the transfer function of the individual filter equation is $a_i/(s + a_i)$, where a_i is referred to as the roll-off frequency.

2.2.1. Design of sliding surface

Consider a two-dimensional compensator with the state vector $\mathbf{q} = [q_1, q_2]'$ as shown in Figure 2:^{12,13,16}

$$\dot{q}_1 = L_{11}q_1 + L_{12}q_2 + \mathbf{N}_1 \boldsymbol{\eta} \quad (26)$$

$$\dot{q}_2 = L_{21}q_1 + L_{22}q_2 + \mathbf{N}_2 \boldsymbol{\eta} + D_2 u + E_{12} \ddot{\mathbf{x}}_g \quad (27)$$

in which $\mathbf{N}_1, \mathbf{N}_2$ are matrices with appropriate dimensions, and $L_{11}, L_{12}, L_{21}, L_{22}, D_2$ and E_{12} are scalars. If feedforward compensation is neglected, then E_{12} is zero. Otherwise, E_{12} is normally chosen to be the element of excitation vector corresponding to the controller location. The sliding surface is expressed in terms of the compensator variables q_1 and q_2 as

$$S = P_1 q_1 + P_2 q_2 = 0 \quad (28)$$

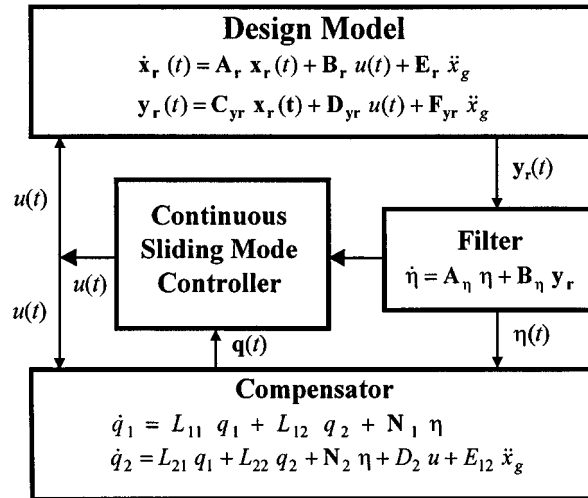


Figure 2. Block diagram of continuous sliding mode control with compensator (CSMC&C)

The sliding surface coefficients P_1 and P_2 , and compensator coefficients, N_1 , N_2 , L_{11} , L_{12} , L_{21} , L_{22} and D_2 , are determined by minimizing an objective function

$$J = E \left[\int_0^\infty \bar{z}_r' Q_z \bar{z}_r + \eta' Q_\eta \eta + q_1' Q_{q_1} q_1 + u_{eq} R_u u_{eq} + \dot{q}_1' R_{\dot{q}_1} \dot{q}_1 dt \right] \quad (29)$$

in which $\bar{z}_r = (C_{zr} x_r + D_{zr} u_{eq})$ and u_{eq} is the equivalent control force. The detail derivations and design producers will be described in the appendix. After minimization, the equivalent control force can be computed by

$$u_{eq} = G\eta + Hq_1 \quad (30)$$

where G and H have been obtained in the process of minimization as described in the appendix.

2.2.2. Design of controller for reaching condition

The controller is designed such that the time derivative of a Lyapunov function $V = 0.5 S' S$ is non-positive at every time instant, i.e. $\dot{V} \leq 0$. The resulting CSMC&C controller is given by^{12,13,16}

$$u = u_{eq} - [M_{c1} + (P_2 D_2)^{-1} \delta P_1] q_1 - [M_{c2} + (P_2 D_2)^{-1} \delta P_2] q_2 - D_2^{-1} E_{12} \ddot{x}_g \quad (31)$$

in which

$$M_{c1} = (P_2 D_2)^{-1} (P_1 L_{12} P_2^{-1} P_1 + P_2 L_{22} P_2^{-1} P_1) \quad (32)$$

$$M_{c2} = (P_2 D_2)^{-1} (P_1 L_{12} + P_2 L_{22}) \quad (33)$$

and δ is the gain margin. The feedforward term, $-D_2^{-1} E_{12} \ddot{x}_g$, in equation (31) can be used to improve the control performance. The control command in equation (31) can be expressed in terms of the feedback loop and feedforward compensation as

$$u = K_b \begin{bmatrix} \eta \\ q_1 \\ q_2 \end{bmatrix} + K_f \ddot{x}_g \quad (34)$$

where the feedback gain matrix, \mathbf{K}_b , and feedforward gain matrix, K_f , are given by

$$\mathbf{K}_b = [\mathbf{G}, H - M_{c1} - (P_2 D_2)^{-1} \delta P_1, -M_{c2} - (P_2 D_2)^{-1} \delta P_2] \quad (35)$$

$$K_f = -D_2^{-1} E_{12} \quad (36)$$

2.2.3. Dynamic output feedback

As observed from equation (34), the feedback loop of the controller u involves the filter output vector η and the compensator variables q_1 and q_2 , which should be computed on-line. Usually, if a hardware low-pass filter is implemented to each measurement, the output η of the filter is considered to be the direct measurement quantities. Then, η is used in equations (26) and (27) to compute q_1 and q_2 . In this case, the dynamic output feedback equation is the two-dimensional compensator equation given in equations (26) and (27). Here, we assume that a software low-pass filter is used; therefore, the first-order filter, equation (21), and the compensator, equations (26) and (27), form a system of dynamic output feedback equations with a $(m + 2)$ -dimensional state vector ξ ,

$$\dot{\xi} = \mathbf{A}_\xi \xi + \mathbf{B}_\xi u + \mathbf{E}_\xi \mathbf{y}_r + \begin{bmatrix} 0 \\ 0 \\ E_{12} \end{bmatrix} \ddot{x}_g \quad (37)$$

where

$$\xi = \begin{bmatrix} \eta \\ q_1 \\ q_2 \end{bmatrix}, \quad \mathbf{A}_\xi = \begin{bmatrix} \mathbf{A}_\eta & 0 & 0 \\ \mathbf{N}_1 & L_{11} & L_{12} \\ \mathbf{N}_2 & L_{21} & L_{22} \end{bmatrix}, \quad \mathbf{B}_\xi = \begin{bmatrix} 0 \\ 0 \\ D_2 \end{bmatrix}, \quad \mathbf{E}_\xi = \begin{bmatrix} \mathbf{B}_\eta \\ 0 \\ 0 \end{bmatrix} \quad (38)$$

Substituting equation (34) into equation (37), one obtains

$$\dot{\xi} = (\mathbf{A}_\xi + \mathbf{B}_\xi \mathbf{K}_b) \xi + \mathbf{E}_\xi \mathbf{y}_r \quad (39)$$

To maintain the stability of equation (39) for the on-line integration, the filter and compensator should be designed such that $(\mathbf{A}_\xi + \mathbf{B}_\xi \mathbf{K}_b)$ is stable. In the simulation for the control performance, \mathbf{y}_r in equation (39) is the actual measurement from the sensors. As observed from equation (39), one advantage of the CSMC&C method is that it involves less on-line computational effort than the use of an observer in CSMC and LQG strategies.

Consequently, the $\mathbf{K}(s)$ matrix for CSMC&C in the block diagram of Figure 1 can be expressed as

$$\mathbf{K}(s) = \mathbf{K}_b (s\mathbf{I} - \mathbf{A}_\xi - \mathbf{B}_\xi \mathbf{K}_b)^{-1} \mathbf{E}_\xi \quad (40)$$

2.3. Control robustness

While the performance of the controller is important, both the robustness of the control performance with respect to system uncertainties, noise and disturbance rejection, and the robustness of the structural stability with respect to system uncertainties are equally important. In particular, for civil engineering applications, uncertainties in damping, stiffness and excitation are quite significant and should be considered. When the control performance is evaluated by the measured output \mathbf{y} and the system is matched (i.e. $\mathbf{E} = \mathbf{B}$), the robustness criterion for the control performance with respect to system uncertainty and disturbance is that the minimum singular value of $\mathbf{P}_{yu}(i\omega) \mathbf{K}(i\omega)$ should be kept as large as possible in the low-frequency range.¹⁷ For the robustness of control performance with respect to noise and the robustness of stability with respect to system uncertainties, the maximum singular value of $\mathbf{P}_{yu}(i\omega) \mathbf{K}(i\omega)$ should be as small as possible in the high-frequency range.¹⁷ For the benchmark problems, the above criterion for the robustness of control performance with respect to system uncertainties and disturbances may not be applicable because our performance is based on \mathbf{z} instead of \mathbf{y} and the system is not matched. However, the criterion for examining the stability robustness and noise rejection is applicable.

Moreover, since the dimensions of $\mathbf{P}_{yu}(i\omega)$ and $\mathbf{K}(i\omega)$ are $(m \times 1)$ and $(1 \times m)$, respectively, the maximum singular value of $\mathbf{P}_{yu}(i\omega) \mathbf{K}(i\omega)$ is equal to the singular value of $\mathbf{K}(i\omega) \mathbf{P}_{yu}(i\omega)$ (a scalar), which is referred to as the loop transfer function of the controller. The plot of $\mathbf{K}(i\omega) \mathbf{P}_{yu}(i\omega)$ in dB versus the frequency for each control design will be presented and compared with the specification of the stability robustness described in Reference 14, i.e. -5 dB for all frequencies above 35 Hz.

For LQG and CSMC controllers in which Kalman–Bucy filters are used as observers, a larger intensity S_w of the measurement noise (or equivalently, a smaller intensity $S_{\ddot{x}_g \ddot{x}_g}$ of excitation) for the observer design will suppress the noise. Since the noise consists of high frequency components, the loop transfer function will be smaller in the high frequency range. In this case, however, the estimation of the state might be degraded. Therefore, a trade-off should be made for the choice of S_w . For CSMC&C controllers that use a first-order low-pass filter for the feedback measurements, the loop transfer function will be smaller in the high-frequency range for smaller \mathbf{A}_η and \mathbf{B}_η . This is because the effect of the measurement noise is less amplified.

3. NUMERICAL SIMULATION AND CONTROL PERFORMANCE

The performances of CSMC and CSMC&C algorithms for two benchmark problems will be demonstrated by numerical simulations using the MATLAB SIMULINK program for the evaluation model. The E1 Centro and Hachinohe earthquake records as well as an artificial earthquake with the nominal Kanai–Tajimi spectrum given in references 14 and 15 ($\omega_g = 37.3$ rad/s, $\zeta_g = 0.3$, and $T_f = 300$ s for the AMD problem, and $\omega_g = 14.5$ rad/s, $\zeta_g = 0.3$ and $T_f = 750$ s for the active tendon problem; for computational simplicity, no maximization over (ω_g, ζ_g) was performed) will be used for simulations. The simulation results based on the LQG control method are also presented for comparison.

3.1. Benchmark Problem No. 1: active mass driver system

The response quantities of the active mass driver system with zero control input, are listed in Table I. Peak response quantities under E1 Centro and Hachinohe earthquake records are shown in columns (2) and (3) of

Table I. Structural response quantities with zero control input

El Centro			Hachinohe			Artificial earthquake				
(1) Quantities	(2) Storey		(3) Storey			(4) Quantities	(5) Storey			
	1	2	3	1	2	3		1	2	3
Active mass driver system										
x_i (cm)	2.09	3.29	3.44	0.96	1.52	1.66	σ_{x_i} (cm)	0.75	1.21	1.28
d_i (cm)	2.09	1.21	0.27	0.96	0.59	0.15	σ_{d_i} (cm)	0.75	0.45	0.08
\ddot{x}_{ai} (g)	3.34	4.62	5.05	1.85	2.17	2.69	$\sigma_{x_{ai}}$ (g)	1.04	1.64	1.75
x_m (cm)		0.25			0.13		σ_{x_m} (cm)		0.09	
\dot{x}_m (cm/s)		10.32			4.84		σ_{x_m} (cm/s)		3.38	
\ddot{x}_{am} (g)		5.43			2.94		$\sigma_{x_{am}}$ (kN)		1.87	
Active tendon system										
x_i (cm)	2.03	4.97	6.57	1.19	2.95	3.85	σ_{x_i} (cm)	0.70	1.80	2.40
d_i (cm)	2.03	3.09	1.81	1.19	1.77	0.95	σ_{d_i} (cm)	0.70	1.11	0.60
\ddot{x}_{ai} (g)	1.08	1.18	1.57	0.43	0.67	0.78	$\sigma_{x_{ai}}$ (g)	0.15	0.37	0.49
x_m (cm)		0.060			0.035		σ_{x_m} (cm)		0.020	
\dot{x}_m (cm/s)		1.072			0.490		σ_{x_m} (cm/s)		0.290	
f (kN)		23.08			13.54		σ_f (kN)		7.87	

the upper part of Table I, whereas the temporal root-mean-square responses under the artificial earthquake, denoted by σ , are shown in column (5) of the upper part of Table I.

With active control, the control output \mathbf{z}_r is chosen to be $\mathbf{z}_r = [d_1, d_2, d_3, \dot{x}_m, \dot{x}_1, \dot{x}_2, \dot{x}_3, \ddot{x}_m, \ddot{x}_{a1}, \ddot{x}_{a2}, \ddot{x}_{a3}, \ddot{x}_{am}]'$ where d_i is the i th interstorey drift. With such a choice of \mathbf{z}_r , the vector \mathbf{F}_z and matrices \mathbf{C}_z and \mathbf{D}_z for the design model are different from those given in Reference 14. However, these can be obtained easily by a simple transformation. For each control strategy, three different design cases (output feedback) are considered; namely, 5-sensor, 3-sensor and 1-sensor. The measured output for these three cases are: (i) 5-sensor; $\mathbf{y}_r = [\dot{x}_m, \ddot{x}_{a1}, \ddot{x}_{a2}, \ddot{x}_{a3}, \ddot{x}_{am}]'$, (ii) 3-sensor; $\mathbf{y}_r = [\ddot{x}_{a1}, \ddot{x}_{a2}, \ddot{x}_{a3}]'$, and (iii) 1-sensor; $\mathbf{y}_r = [\ddot{x}_{a3}]'$. The (10×10) design model constructed by Spencer *et al.*¹⁴ was used for LQG controllers, whereas another (10×10) design model constructed by the 'balreal' and 'modred' functions in MATLAB CONTROL SYSTEM TOOLBOX was used for CSMC and CSMC&C controllers. The practical limitations, such as the maximum control command, maximum driver acceleration and maximum actuator stroke, and the simulation guidelines were given in Reference 14. All the controller are designed to utilize as much as possible the full capacity of the actuator without violating the constraints.

For the LQG controllers, the control output \mathbf{z}_r and the control command u are tuned as follows: (i) 5-sensor case; $\mathbf{Q} = \text{diag}[130, 100, 100, 0, 0, 0, 0, 0, 1, 1, 10, 62]$, $R = 50$, (ii) 3-sensor case; $\mathbf{Q} = \text{diag}[32, 10, 10, 0, 0, 0, 0, 0, 1, 1, 1, 5]$, $R = 13$, and (iii) 1-sensor case; $\mathbf{Q} = \text{diag}[50, 43, 43, 0, 0, 0, 0, 0, 1, 1, 10, 12]$, $R = 40$. For the design of observers, $\gamma = S_{\ddot{x}_e \ddot{x}_e} / S_{v_i v_i} = 5$ is used. The controllers are designed such that the magnitude of the loop transfer function is below -5 dB for frequencies above 35 Hz. As explained earlier, this can be achieved by use of a smaller γ ; however, a smaller γ may degrade the estimation of the state. After extensive simulations, a value $\gamma = 5$ is used. The loop transfer functions $\mathbf{K}(i\omega) \mathbf{P}_y(i\omega)$, for the LQG method are shown in Figure 3(a), in which the results for the 5-sensor, 3-sensor and 1-sensor cases are denoted by the solid curve, dashed-dot curve and dashed curve, respectively. J_1 to J_{10} for the evaluation model are presented in columns (2), (6) and (10) of Table II for 5-sensor, 3-sensor and 1-sensor cases, respectively. The root-mean-square command voltage under the stochastic earthquake is denoted by σ_u in Table II, whereas the maximum command voltage under E1 Centro and Hachinohe earthquakes are denoted by $|u(t)|$ in Table II. Under E1 Centro earthquake, the time history of the first-storey drift, d_1 , for the 5-sensor case are presented in Figure 4(a), in which the dotted curve and the solid curve represent the response quantity without control (zero control input) and that using LQG controller, respectively.

For CSMC controllers, the feedforward compensation is ignored for the fairness of comparisons. The design parameters for controllers are as follows: (i) 5-sensor case; $\mathbf{Q} = \text{diag}[1600, 1100, 1100, 0, 0, 0, 0, 0, 110, 10, 15, 15, 1]$, $\delta = 40$, (ii) 3-sensor case; $\mathbf{Q} = \text{diag}[1100, 1100, 1100, 0, 0, 0, 0, 0, 165, 10, 15, 15, 1]$, $\delta = 40$ and (iii) 1-sensor case; $\mathbf{Q} = \text{diag}[1500, 1100, 1100, 0, 10, 0, 0, 0, 100, 10, 15, 15, 20]$, $\delta = 40$. For the observer design, we choose $\gamma = S_{\ddot{x}_e \ddot{x}_e} / S_{v_i v_i} = 5$ such that the loop transfer function is smaller than -5 dB for frequencies above 35 Hz. The loop transfer functions for the CSMC method are presented in Figure 3(b), in which the results for 5-sensor, 3-sensor and 1-sensor cases are denoted by the solid curve, dashed-dot curve and dashed curve, respectively. J_1 to J_{10} as well as σ_u and $|u(t)|$ for the evaluation model are presented in columns (3), (7) and (11) of Table II for 5-sensor, 3-sensor and 1-sensor cases, respectively. For the 5-sensor case using CSMC control, the time history of the first-storey drift, d_1 , under E1 Centro earthquake is presented in Figure 4(b) by the solid curve, whereas the dotted curve represents the corresponding response without control. The time history of the sliding surface S is plotted in Figure 4(c). As observed from Figure 4(c), the sliding surface $S = 0$ is not maintained because (i) the feedforward compensation in equation (9) has been ignored, and (ii) the estimation of state \mathbf{x}_t from an observer is required in the computation of the control command. However, the stability of S is always guaranteed.

The design parameters for CSMC&C controllers are as follows: (i) 5-sensor case; $\mathbf{A}_\eta = -7\mathbf{I}_5$, $\mathbf{B}_\eta = 7\mathbf{I}_5$, where \mathbf{I}_m is an $(m \times m)$ identity matrix, $\mathbf{Q}_z = \text{diag}[6000, 6000, 6000, 0, 0, 0, 0, 120, 1, 1, 1, 800]$, $\mathbf{Q}_{q_1} = 1$, $\mathbf{Q}_\eta = \text{diag}[0, 120, 120, 120, 0]$, $R_u = 0.1$, $R_{q_1} = 0.1$, $L_{12} = -1$, $L_{22} = -0.001$, $P_1 = 1$, $P_2 = 1000$, $D_2 = 1$ and $\delta = 10^7$, (ii) 3-sensor case; $\mathbf{A}_\eta = -10\mathbf{I}_3$, $\mathbf{B}_\eta = 10\mathbf{I}_3$, $\mathbf{Q}_z = \text{diag}[800, 800, 800, 0, 0, 0, 0, 50, 0, 0, 0, 60]$, $\mathbf{Q}_\eta = \text{diag}[100, 100, 100]$ and all other parameters are identical to case (i), and (iii) 1-sensor case; $\mathbf{A}_\eta = -10$,

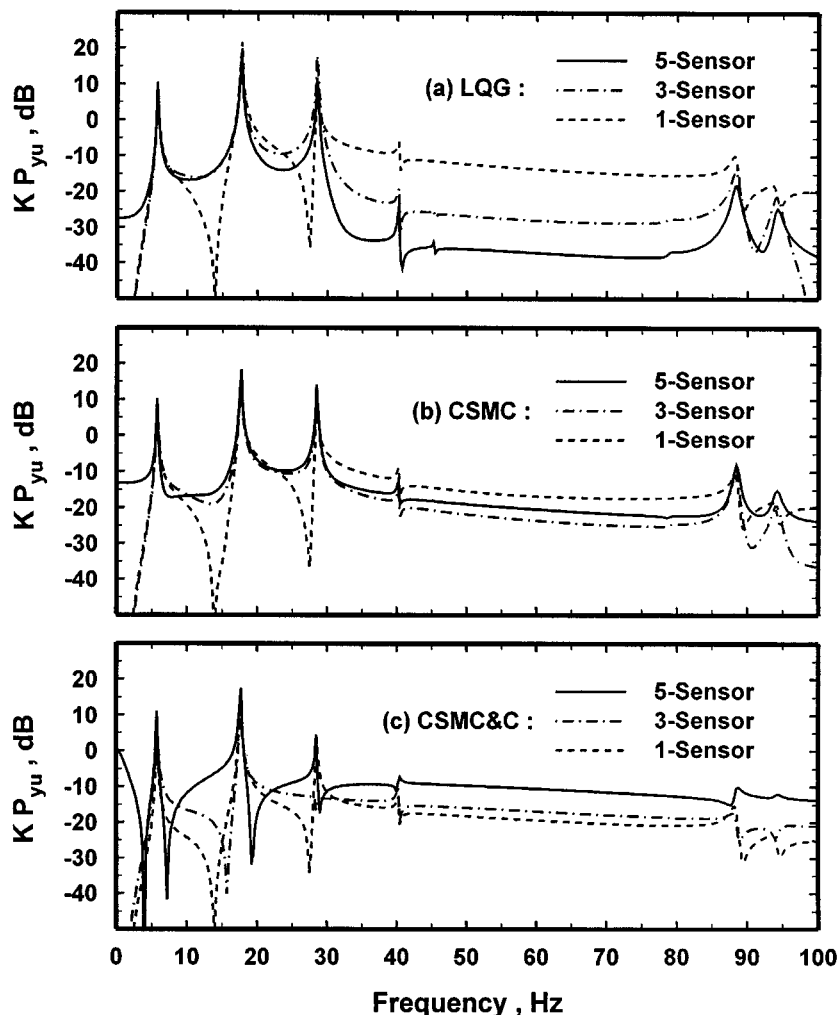


Figure 3. Loop transfer functions for active mass driver system for: (a) LQG; (b) CSMC; and (c) CSMC&C methods

$\mathbf{B}_\eta = 10$, $\mathbf{Q}_z = \text{diag}[6000, 700, 2000, 0, 0, 0, 0, 100, 0, 0, 0, 100]$, $\mathbf{Q}_\eta = 100$ and all other parameters are identical to case (i). Note that the compensator coefficients \mathbf{N}_1 , \mathbf{N}_2 , L_{11} and L_{21} were computed from the design parameters above by minimizing equation (29) as presented in appendix (see also References 12 and 16). For the fairness of comparisons, the feedforward part is ignored, i.e. $E_{12} = 0$. The choice of \mathbf{A}_η and \mathbf{B}_η depends on whether the requirement for the loop transfer function can be satisfied. As mentioned earlier, the requirement can be satisfied easily by choosing smaller \mathbf{A}_η and \mathbf{B}_η . However, extensive simulation results indicate that it is difficult to adjust the control command to be more than 1 V if smaller \mathbf{A}_η and \mathbf{B}_η are used. Therefore, a trade-off was made to choose the above values for \mathbf{A}_η and \mathbf{B}_η . The loop transfer functions are plotted in Figure 3(c), in which the results for 5-sensor, 3-sensor and 1-sensor cases are denoted by the solid curve, dashed-dot curve and dashed curve, respectively. J_1 to J_{10} as well as σ_u and $|u(t)|$ for the evaluation model are presented in columns (4), (8) and (12) of Table II. Note that we cannot adjust the control command to be more than 1 V for the 1-sensor case because of the limitation of such a configuration. For the 5-sensor case using CSMC&C control, the time history of the first-storey drift under E1 Centro earthquake is presented in Figure 4(d) by the solid curve, whereas the dotted curve represents the response without control. The time

Table II. Comparison of evaluation criteria for LQG, CSMC, and CSMC&C controllers for active mass driver system

Quantities	LQG		CSMC		CSMC&C	
Five-sensor case, $\mathbf{y}_r = [x_m, \ddot{x}_{a1}, \ddot{x}_{a2}, \ddot{x}_{a3}, \ddot{x}_{am}]'$						
(1)	(2)		(3)		(4)	
J_1	0.1878		0.1979		0.2114	
J_2	0.2846		0.2936		0.3183	
J_3	0.8444		0.8221		0.7783	
J_4	0.8259		0.8042		0.7560	
J_5	0.8327		0.7775		0.6443	
σ_u (Vs)	0.2710		0.2668		0.2637	
$\sigma_{x_{am}}$ (g)	1.4905		1.3917		1.1534	
σ_{x_m} (cm)	1.1062		1.0770		1.0196	
	E1 Centro	Hachinohe	E1 Centro	Hachinohe	E1 Centro	Hachinohe
J_6	0.3083	0.3779	0.3077	0.3738	0.3275	0.3757
J_7	0.4725	0.6616	0.4730	0.6674	0.6201	0.6287
J_8	1.2479	1.6240	1.2338	1.6832	1.1971	1.7292
J_9	1.2098	1.4811	1.2183	1.4903	1.2097	1.4550
J_{10}	1.1078	1.6491	1.0749	1.5673	1.1071	1.2821
max $ u $ (Vs)	1.1601	0.7539	1.1481	0.7818	1.1612	0.8087
max $ \ddot{x}_{am} $ (g)	5.5942	4.2546	5.4282	4.0435	5.5908	3.3077
max $ x_m $ (cm)	4.2056	2.6958	4.1578	2.7941	4.0343	2.8705
Three-sensor case, $\mathbf{y}_r = [\ddot{x}_{a1}, \ddot{x}_{a2}, \ddot{x}_{a3}]$						
(5)	(6)		(7)		(8)	
J_1	0.1943		0.1963		0.1948	
J_2	0.2956		0.2956		0.2939	
J_3	0.8126		0.8110		0.8286	
J_4	0.7984		0.7970		0.7945	
J_5	0.8287		0.8004		0.7409	
σ_u (Vs)	0.2567		0.2599		0.2742	
$\sigma_{x_{am}}$ (g)	1.4834		1.4372		1.3261	
σ_{x_m} (cm)	1.0645		1.0625		1.0855	
	E1 Centro	Hachinohe	E1 Centro	Hachinohe	E1 Centro	Hachinohe
J_6	0.3164	0.3818	0.3112	0.3760	0.3068	0.3700
J_7	0.4888	0.6691	0.4888	0.6695	0.5559	0.6269
J_8	1.1783	1.5022	1.2051	1.5819	1.2415	1.8663
J_9	1.1608	1.4376	1.1870	1.4060	1.2345	1.5739
J_{10}	1.1026	1.7515	1.1204	1.4647	1.1817	1.5217
max $ u $ (Vs)	1.0989	0.7071	1.1267	0.7350	1.1906	0.8686
max $ \ddot{x}_{am} $ (g)	5.5680	3.5189	5.6581	3.7790	5.9677	3.9260
max $ x_m $ (cm)	3.9710	2.4937	4.0613	2.6260	4.1838	3.0981
One-sensor case, $\mathbf{y}_r = [\ddot{x}_{a3}]$						
(9)	(10)		(11)		(12)	
J_1	0.2112		0.2114		0.2661	
J_2	0.3234		0.3235		0.4093	
J_3	0.7696		0.7650		0.5490	
J_4	0.7600		0.7524		0.5428	
J_5	0.7805		0.7677		0.5309	
σ_u (Vs)	0.2473		0.2454		0.1710	
$\sigma_{x_{am}}$ (g)	1.3971		1.3741		1.9503	
σ_{x_m} (cm)	1.0082		1.0022		0.7192	

Table II. (Continued)

Quantities	LQG		CSMC		CSMC&C	
	E1 Centro	Hachinohe	E1 Centro	Hachinohe	E1 Centro	Hachinohe
J_6	0.3196	0.3844	0.3167	0.3784	0.3739	0.4179
J_7	0.4957	0.6915	0.5168	0.6824	0.7188	0.7001
J_8	1.1451	1.3643	1.1360	1.4741	0.6983	0.9366
J_9	1.1442	1.5644	1.1306	1.3974	0.7241	0.9154
J_{10}	1.1706	1.8799	1.1817	1.4123	0.8675	0.9064
$\max u $ (Vs)	1.0638	0.6517	1.0607	0.6844	0.6984	0.4405
$\max \ddot{x}_{am} $ (g)	5.9118	4.8503	5.9677	3.6438	4.3806	2.3386
$\max x_m $ (cm)	3.8590	2.2647	3.8283	2.4469	2.3531	1.5548

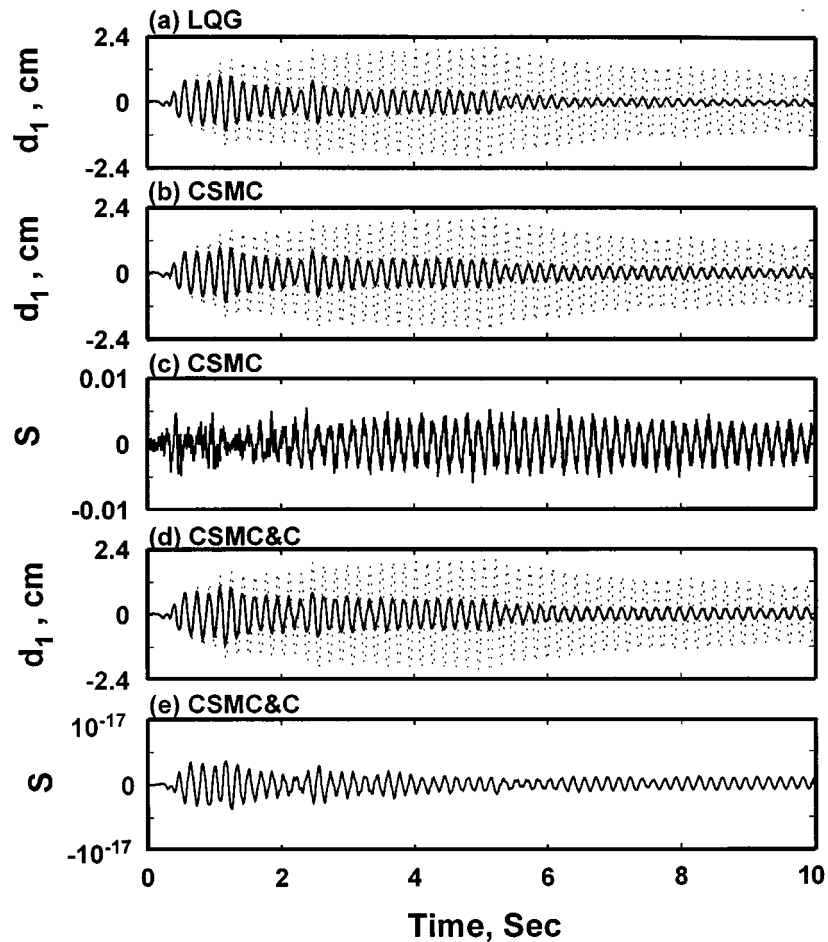


Figure 4. Time histories of first storey drift and sliding surface for active mass driver system under El Centro Earthquake (5-sensor case) using LQG, CSMC and CSMC&C controllers

history of the sliding surface S is plotted in Figure 4(e). As observed from Figure 4(e), the sliding surface motion $S = 0$ is well maintained, since the control command in equation (31) always guarantees $\dot{V} \leq 0$.

As observed from Table II, the control performances for three control methods, i.e. LQG, CSMC and CSMC&C, are quite comparable.

3.2. Benchmark problem No. 2: active tendon system

The response quantities of the active tendon system with zero control command are listed in the lower part of Table I. For active control, the control output \mathbf{z}_r of the active tendon system is chosen as $\mathbf{z}_r = [d_1, d_2, d_3, x_p, \dot{x}_1, \dot{x}_2, \dot{x}_3, \dot{x}_p, \ddot{x}_{a1}, \ddot{x}_{a2}, \ddot{x}_{a3}, f]'$ in which d_i is the i th interstorey drift. For each control strategy, three different design cases are considered; namely, 5-sensor, 3-sensor and 1-sensor. The measured output for these cases are: (i) 5-sensor; $\mathbf{y}_r = [x_p, \ddot{x}_{a1}, \ddot{x}_{a2}, \ddot{x}_{a3}, f]'$, (ii) 3-sensor; $\mathbf{y}_r = [\ddot{x}_{a1}, \ddot{x}_{a2}, \ddot{x}_{a3}]'$ for LQG and CSMC, and $\mathbf{y}_r = [x_p, \ddot{x}_{a3}, f]'$ for CSMC&C, and (iii) 1-sensor; $\mathbf{y}_r = [\ddot{x}_{a3}]$ for LQG and CSMC, and $\mathbf{y}_r = [f]$ for CSMC&C. A (12×12) design model constructed by the 'balreal' and 'modred' functions in MATLAB CONTROL SYSTEM TOOLBOX was used for LQG and CSMC controllers. Another (12×12) design model used for CSMC&C controllers is obtained by making a balanced transformation of the evaluation model and reducing the system by keeping the same eigenproperties of the first 12 complex modes.^{16,18} The limitations, such as the maximum control command and actuator stroke, and the simulation guidelines were given in Reference 15. All the controllers are designed to utilize as much as possible the full capacity of the actuator (i.e. control efforts) without violating the constraints.

For the LQG controllers, the control output \mathbf{z}_r and the control command u are tuned as follows: (i) 5-sensor case; $\mathbf{Q} = \text{diag}[1, 1, 1, 0, 0, 0, 0, 0, 1, 1, 1, 6]$, $R = 4$, (ii) 3-sensor case; $\mathbf{Q} = \text{diag}[1, 1, 1, 0, 0, 0, 0, 0, 1, 1, 1, 6]$, $R = 4$ and (iii) 1-sensor case; $\mathbf{Q} = \text{diag}[1, 1, 1, 0, 0, 0, 0, 0, 1, 1, 1, 6]$, $R = 3$. For the observer, $\gamma = S_{\ddot{x}_g \ddot{x}_g} / S_{v_i v_i} = 0.5$ used such that the magnitude of the loop transfer function is less than -5 dB for frequencies above 35 Hz. The loop transfer functions, $\mathbf{K}(i\omega) \mathbf{P}_{yu}(i\omega)$, for the LQG method are shown in Figure 5(a), in which the 5-sensor, 3-sensor and 1-sensor cases are denoted by the solid curve, dashed-dot curve and dashed curve, respectively. J_1 to J_{10} as well as σ_u and $|u(t)|$ for the evaluation model are presented in columns (2), (6) and (10) of Table III for 5-sensor, 3-sensor and 1-sensor cases, respectively. For the 5-sensor case using LQG control, the time history of the third-storey drift under E1 Centro earthquake is presented in Figure 6(a) by the solid curve, whereas the dotted curve represents the response without control.

For CSMC controllers, the control parameters are given as follows: (i) 5-sensor case; $\mathbf{Q} = \text{diag}[10, 10, 10, 80, 0, 0, 0, 0, 100, 10, 10, 110]$, $\delta = 80$, (ii) 3-sensor case; $\mathbf{Q} = \text{diag}[10, 10, 10, 80, 0, 0, 0, 0, 100, 10, 10, 110]$, $\delta = 80$, and (iii) 1-sensor case; $\mathbf{Q} = \text{diag}[10, 10, 10, 80, 0, 0, 0, 0, 100, 10, 10, 110]$, $\delta = 80$. For the observer design for all three cases, we consider $\gamma = S_{\ddot{x}_g \ddot{x}_g} / S_{v_i v_i} = 5$ such that the criterion for the stability robustness is satisfied. The loop transfer functions for CSMC controllers are shown in Figure 5(b), in which the 5-sensor, 3-sensor and 1-sensor cases are denoted by the solid curve, dashed-dot curve and dashed curve, respectively. J_1 to J_{10} as well as σ_u and $|u(t)|$ for the evaluation model are presented in columns (3), (7) and (11) of Table III for 5-sensor, 3-sensor and 1-sensor cases, respectively. For the 5-sensor case using CSMC control, the time history of the third-story drift under E1 Centro earthquake is presented in Figure 6(b) by the solid curve, whereas the dotted curve represents the response without control. The time history of the sliding surface S for the 5-sensor case is also plotted in Figure 6(c). As observed from Figure 6(c), the sliding surface motion $S = 0$ is not maintained because: (i) the feedforward compensation in Eq. (9) has been ignored, and (ii) the estimation of the state, \mathbf{x}_r , from an observer is required in the computation of the control command. However, the stability of S is always guaranteed. As observed from Table III, the control performances for both LQG and CSMC controllers are remarkable even using only one acceleration sensor on the top floor.

For CSMC&C controllers, the parameters for the filter are chosen to be $\mathbf{A}_\eta = -10\mathbf{I}_m$ and $\mathbf{B}_\eta = 10\mathbf{I}_m$, where m is the number of sensor. The design parameters are given as follows: (i) 5-sensor case; $\mathbf{Q}_z = \text{diag}[10, 10, 10, 0, 0, 0, 0, 0, 10, 10, 10, 20]$, $\mathbf{Q}_\eta = \text{diag}[0, 0, 0, 0, 0, 0]$, $\mathbf{Q}_{q1} = 1$, $R_u = 30$, $R_{\dot{q}_1} = 0.1$, $L_{12} = 0.1$, $L_{22} = -2$, $P_1 = 1$, $P_2 = 1$, $D_2 = 1$ and $\delta = 100$, (ii) 3-sensor case; $\mathbf{Q}_z = \text{diag}[1, 1, 1, 0, 0, 0, 0, 0, 1, 1, 1, 150]$,

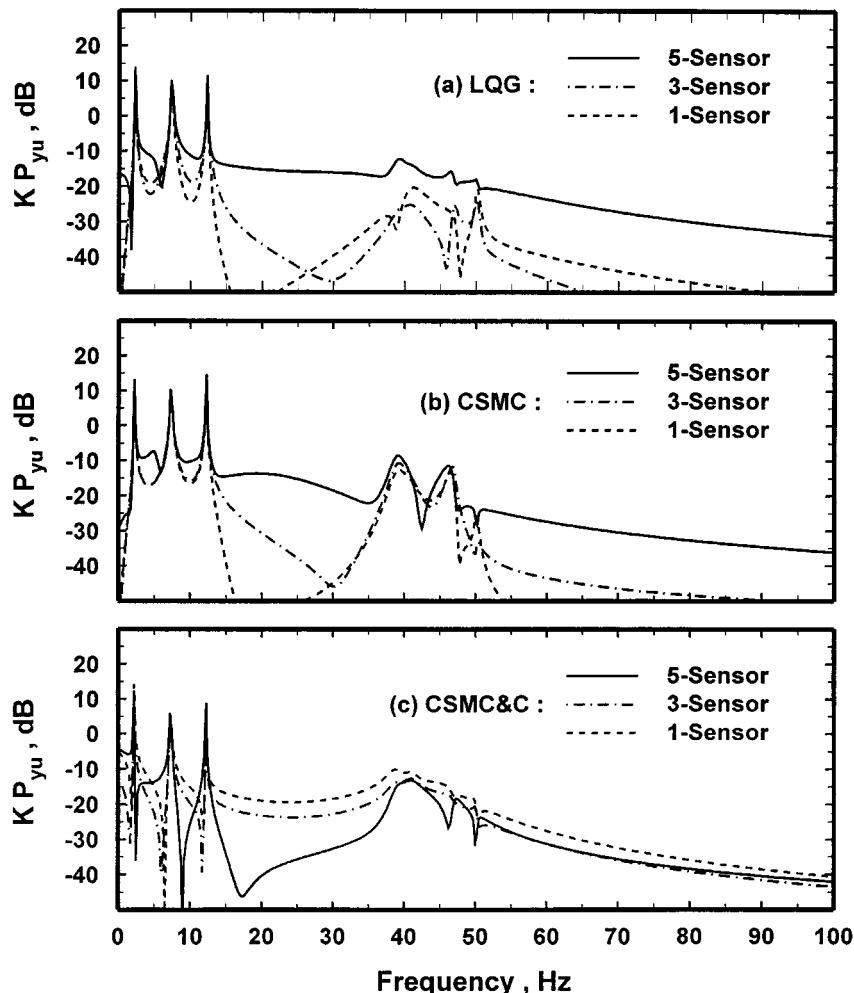


Figure 5. Loop transfer functions for active tendon system for: (a) LQG; (b) CSMC; and (c) CSMC&C methods

$\mathbf{Q}_\eta = \text{diag}[0, 0, 0]$, $\mathbf{Q}_{q_1} = 1$, $R_u = 200$, $R_{q_1} = 0.1$, $L_{12} = 0.1$, $L_{22} = -2$, $P_1 = 1$, $P_2 = 1$, $D_2 = 1$ and $\delta = 100$, (iii) 1-sensor case; $\mathbf{Q}_z = \text{diag}[1, 1, 1, 0, 0, 0, 0, 0, 1, 1, 1, 10]$, $\mathbf{Q}_\eta = 0$, $\mathbf{Q}_{q_1} = 1$, $R_u = 10$, $R_{q_1} = 0.1$, $L_{12} = 0.1$, $L_{22} = -2$, $P_1 = 1$, $P_2 = 1$, $D_2 = 1$ and $\delta = 100$. As in the active mass driver system, a smaller \mathbf{A}_η and \mathbf{B}_η can satisfy the criterion for stability robustness. The loop transfer functions of CSMC&C controllers are plotted in Figure 5(c) in which the solid curve, dashed-dot curve and dashed curve denote the loop transfer functions for the 5-sensor, 3-sensor and 1-sensor cases, respectively. J_1 to J_{10} as well as σ_u and $|u(t)|$ for the evaluation model are presented in columns (4), (8) and (12) of Table III for 5-sensor, 3-sensor and 1-sensor cases, respectively. For the 5-sensor case using CSMC&C control, the time history of the third-storey drift under E1 Centro earthquake is presented in Figure 6(d) by the solid curve, whereas the dotted curve represents the response without control. The time history of the sliding surface S for the 5-sensor case is also plotted in Figure 6(e). As observed from Figure 6(e), the sliding surface motion $S = 0$ is well maintained, since the control command in equation (31) always guarantees $\dot{V} \leq 0$.

It is observed from Table III that the control performances of CSMC controllers are comparable to those of LQG controllers. Although the performance of CSMC&C is slightly worse than LQG and CSMC;

Table III. Comparison of evaluation criteria for LQG, CSMC, and CSMC&C controllers for active tendon system

Quantities	LQG		CSMC		CSMC&C	
Five-sensor case, $\mathbf{y}_r = [x_p, \ddot{x}_{a1}, \ddot{x}_{a2}, \ddot{x}_{a3}, f]'$						
(1)	(2)		(3)		(4)	
J_1	0.1646		0.1572		0.1727	
J_2	0.3472		0.3387		0.3669	
J_3	0.0329		0.0308		0.0317	
J_4	0.0343		0.0328		0.0307	
J_5	0.0089		0.0095		0.0097	
σ_u (Vs)	0.5978		0.5780		0.5811	
σ_f (kN)	2.5703		2.7360		2.7969	
σ_{x_p} (cm)	0.0771		0.0721		0.0743	
	E1 Centro	Hachinohe	E1 Centro	Hachinohe	E1 Centro	Hachinohe
J_6	0.2506	0.3223	0.2421	0.3157	0.2583	0.3245
J_7	0.5252	0.8514	0.4942	0.8437	0.4974	0.8097
J_8	0.0491	0.0662	0.0463	0.0674	0.0520	0.0611
J_9	0.0539	0.0677	0.0594	0.0729	0.0431	0.0549
J_{10}	0.0350	0.0269	0.0373	0.0295	0.0382	0.0266
max $ u $ (Vs)	2.4737	1.9540	2.4188	2.0424	2.6109	1.8224
max $ f $ (kN)	10.1196	7.7831	10.7916	8.5367	11.0252	7.6821
max $ x_p $ (cm)	0.3166	0.2502	0.2989	0.2548	0.3355	0.2311
Three-sensor case, $\mathbf{y}_r = [\ddot{x}_{a1}, \ddot{x}_{a2}, \ddot{x}_{a3}]'$						
(5)	(6)		(7)		(8)	
J_1	0.1681		0.1568		0.1831	
J_2	0.3545		0.3377		0.3802	
J_3	0.0328		0.0312		0.0367	
J_4	0.0341		0.0331		0.0370	
J_5	0.0091		0.0094		0.0090	
σ_u (Vs)	0.5948		0.5846		0.6495	
σ_f (kN)	2.6187		2.7268		2.6008	
σ_{x_p} (cm)	0.0768		0.0730		0.0858	
	E1 Centro	Hachinohe	E1 Centro	Hachinohe	E1 Centro	Hachinohe
J_6	0.2559	0.3276	0.2408	0.3166	0.2705	0.3333
J_7	0.5316	0.8603	0.4935	0.8438	0.5522	0.8126
J_8	0.0495	0.0606	0.0468	0.0675	0.0559	0.0631
J_9	0.0515	0.0666	0.0602	0.0737	0.0496	0.0610
J_{10}	0.0354	0.0271	0.0375	0.0294	0.0352	0.0242
max $ u $ (Vs)	2.4669	1.7905	2.4220	2.0457	2.7256	1.8084
max $ f $ (kN)	10.2325	7.8390	10.8343	8.4854	10.1765	6.9796
max $ x_p $ (cm)	0.3196	0.2292	0.3015	0.2553	0.3606	0.2378
One-sensor case, $\mathbf{y}_r = [\ddot{x}_{a3}]'$						
(9)	(10)		(11)		(12)	
J_1	0.1620		0.1575		0.1905	
J_2	0.3409		0.3390		0.3927	
J_3	0.0347		0.0312		0.0394	
J_4	0.0362		0.0330		0.0398	
J_5	0.0086		0.0094		0.0090	
σ_u (Vs)	0.6297		0.5848		0.6930	
σ_f (kN)	2.4967		2.7269		2.5927	
σ_{x_p} (cm)	0.0812		0.0731		0.0922	

Table III. (Continued)

Quantities	LQG		CSMC		CSMC&C	
	E1 Centro	Hachinohe	E1 Centro	Hachinohe	E1 Centro	Hachinohe
J_6	0.2497	0.3256	0.2404	0.3190	0.2798	0.3367
J_7	0.5188	0.8578	0.4888	0.8357	0.5748	0.8162
J_8	0.0531	0.0640	0.0473	0.0666	0.0588	0.0640
J_9	0.0558	0.0717	0.0563	0.0715	0.0530	0.0648
J_{10}	0.0346	0.0273	0.0373	0.0293	0.0354	0.0233
max $ u $ (Vs)	2.6677	1.8869	2.3976	2.0157	2.8488	1.8233
max $ f $ (kN)	10.0112	7.9026	10.7788	8.4632	10.2429	6.7449
max $ x_p $ (cm)	0.3426	0.2421	0.3049	0.2516	0.3795	0.2421

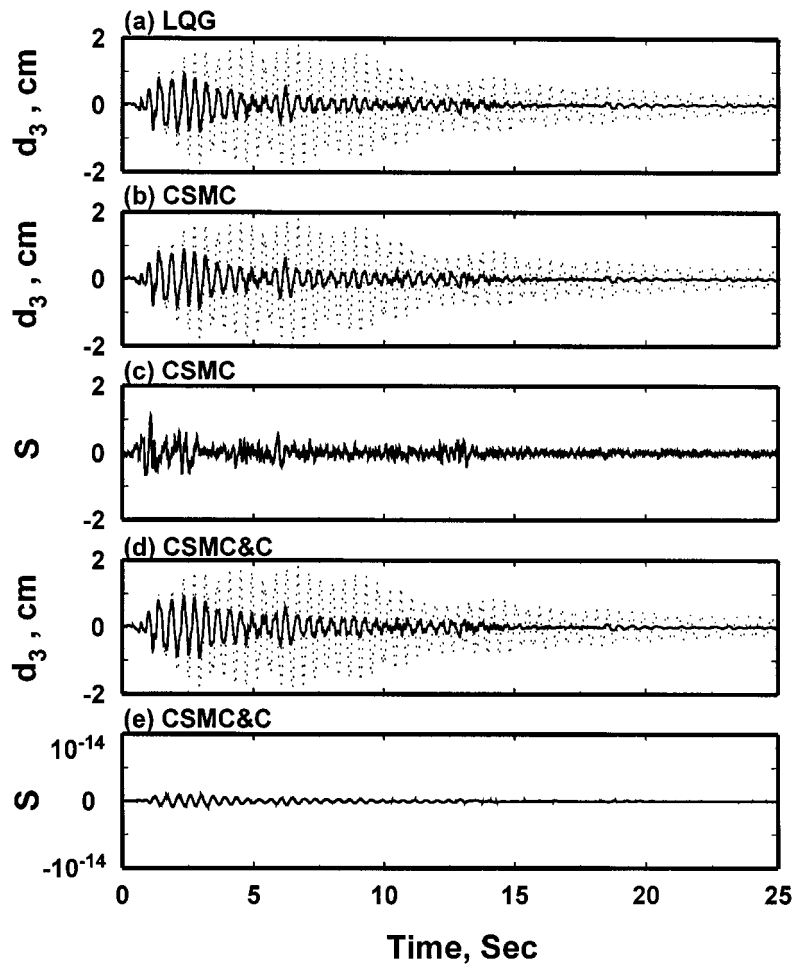


Figure 6. Time histories of third-storey drift and sliding surface for active tendon system under El Centro Earthquake (5-sensor case) using LQG, CSMC and CSMC&C controllers

however, it is easier to implement CSMC&C controllers because the dimension of the dynamic output feedback equation is smaller.

4. CONCLUSIONS

The methods of continuous sliding mode control (CSMC) and continuous sliding mode control with a compensator (CSMC&C) have been applied to two benchmark models. Due to the specific identification scheme used in the benchmark problem in which the state variables are fictitious and the output measurement y involves both the control signal and the earthquake excitation, static output feedback controllers are not applicable and therefore the design of CSMC and CSMC&C controllers becomes more involved. Likewise, the performances of CSMC and CSMC&C controllers may have been compromised. As a result, an observer is used for CSMC controllers, whereas a low-pass filter is introduced for each measurement in CSMC&C controllers.

The purpose of introducing filters in CSMC&C is to transform the benchmark formulations into strictly proper forms such that the framework of static output feedback can be used. The design procedures for CSMC&C involve LQR static output feedback such that numerical iterations are required. To obtain a convergent solution, we start with a larger weighting R_u for the control effort u_{eq} , and then reduce R_u gradually. The solution for the previous R_u is used as the initial trial for the next R_u value. Further, the compensator parameters L_{12} and L_{22} were assigned such that not only the compensator system matrix \mathbf{L} is stable but also the open-loop system of compensator is stable. As a result, the design procedures and computational efforts involved in designing a CSMC&C controller is much more involved than that of CSMC and LQG controllers. However, an advantage of the CSMC&C controllers is that the on-line computational effort is reduced because the dimension (i.e. $m + 2$) of filters and compensator is smaller than that of an observer.

The robustness of stability and noise rejection has been presented by plotting the loop transfer function of the controller. To ensure a larger stability margin, the loop transfer function should be as small as possible in the high frequency range. For this purpose, a trade-off has been made for the selection of the intensity of white noise excitation and measurement noise for LQG and CSMC methods. For the CSMC&C method, the stability margin can be enlarged sufficiently by choosing smaller \mathbf{A}_η and \mathbf{B}_η . Simulation results indicate that the performances of CSMC and CSMC&C controllers are quite comparable to that of the LQG method.

APPENDIX: DERIVATIONS AND DESIGN PROCEDURES FOR SLIDING SURFACE OF CSMC&C

To confine the response trajectory on the sliding surface, the conditions, $S = 0$ and $\dot{S} = 0$, should be satisfied. Then, it follows from equation (28) that

$$q_2 = -P_2^{-1}P_1q_1 \quad (41)$$

provided that P_2 is invertible, and

$$\dot{S} = P_1 \dot{q}_1 + P_2 \dot{q}_2 = 0 \quad (42)$$

Substituting equations (41), (26) and (27) into equation (42), one obtains the control force u , denoted by u_{eq} , as

$$u_{eq} = \mathbf{G}\eta + Hq_1 \quad (43)$$

in which

$$\mathbf{G} = -(P_2 D_2)^{-1} (P_1 N_1 + P_2 N_2) \quad (44)$$

$$H = -(P_2 D_2)^{-1} [P_1 (L_{11} - L_{12} P_2^{-1} P_1) + P_2 (L_{21} - L_{22} P_2^{-1} P_1)] \quad (45)$$

where u_{eq} is referred to as the equivalent control force, that is the control force needed to confine (or maintain) the system on the sliding surface $S = 0$, once the system trajectory reaches $S = 0$.

Substitution of the equivalent control u_{eq} into the augmented design model, equation (22), the closed-loop system of the structure on the sliding surface is given by

$$\dot{\tilde{\mathbf{x}}}_r = \tilde{\mathbf{A}}_r \tilde{\mathbf{x}}_r + \tilde{\mathbf{B}}_r u_{eq} \quad (46)$$

in which the excitation $\tilde{\mathbf{W}}$ has been neglected. Note that in the design of the sliding surface, the external excitation is neglected; however, it is taken into account in the design of the controller. Substitution of q_2 given by equation (41) into equation (27) leads to the compensator dynamics for q_1 on the sliding surface as

$$\dot{q}_1 = (L_{11} - L_{12} P_2^{-1} P_1) q_1 + N_1 y \quad (47)$$

Thus, the entire structure-compensator system on the sliding surface defined by equation (46) and (47) can be cast into an augmented state equation of strictly proper form with a $(r + m + 1)$ -dimensional state vector $\bar{\mathbf{Z}}$,

$$\dot{\bar{\mathbf{Z}}} = \bar{\mathbf{A}} \bar{\mathbf{Z}} + \bar{\mathbf{B}} \bar{u} \quad (48)$$

$$\bar{y} = \bar{\mathbf{C}} \bar{\mathbf{Z}} \quad (49)$$

in which

$$\bar{\mathbf{Z}} = \begin{bmatrix} \tilde{\mathbf{x}}_r \\ q_1 \end{bmatrix}, \quad \bar{y} = \begin{bmatrix} \eta \\ q_1 \end{bmatrix}, \quad \bar{\mathbf{A}} = \begin{bmatrix} \tilde{\mathbf{A}}_r & 0 \\ 0 & 0 \end{bmatrix}, \quad \bar{\mathbf{B}} = \begin{bmatrix} \tilde{\mathbf{B}}_r & 0 \\ 0 & 1 \end{bmatrix}, \quad \bar{u} = \begin{bmatrix} u_{eq} \\ \dot{q}_1 \end{bmatrix}, \quad \bar{\mathbf{C}} = \begin{bmatrix} \tilde{\mathbf{C}}_{yr} & 0 \\ 0 & 1 \end{bmatrix} \quad (50)$$

and equations (43) and (47) can be combined as

$$\bar{u} = \bar{\mathbf{G}} \bar{y} \quad (51)$$

in which

$$\bar{\mathbf{G}} = \begin{bmatrix} \mathbf{G} & H \\ N_1 & L_{11} - L_{12} P_2^{-1} P_1 \end{bmatrix} \quad (52)$$

P_1 and P_2 as well as the compensator characteristics will be determined from the augmented system defined by equations (48) and (49). For the augmented system in equations (48) and (49) with the static output control in equation (51), the gain matrix $\bar{\mathbf{G}}$ can be obtained by minimizing a quadratic performance index, equation (29). Equation (29) can be further rearranged into the typical form of

$$J = E \left\{ \int_0^\infty [\bar{\mathbf{Z}}' \quad \bar{u}'] \begin{bmatrix} \bar{\mathbf{Q}} & \bar{\mathbf{S}} \\ \bar{\mathbf{S}}' & \bar{\mathbf{R}} \end{bmatrix} \begin{bmatrix} \bar{\mathbf{Z}} \\ \bar{u} \end{bmatrix} dt \right\} \quad (53)$$

in which

$$\bar{\mathbf{Q}} = \begin{bmatrix} \mathbf{C}_z' \mathbf{Q}_z \mathbf{C}_z & 0 & 0 \\ 0 & \mathbf{Q}_\eta & 0 \\ 0 & 0 & \mathbf{Q}_{q_1} \end{bmatrix}, \quad \bar{\mathbf{R}} = \begin{bmatrix} \mathbf{D}_z' \mathbf{Q}_z \mathbf{C}_z + \mathbf{R}_u & 0 \\ 0 & \mathbf{R}_{\dot{q}_1} \end{bmatrix}, \quad \bar{\mathbf{S}} = \begin{bmatrix} \mathbf{C}_z' \mathbf{Q}_z \mathbf{D}_z & 0 \\ 0 & 0 \\ 0 & 0 \end{bmatrix} \quad (54)$$

As observed from equation (53), the coupled weighting matrix $\bar{\mathbf{S}}$ between $\bar{\mathbf{Z}}$ and $\bar{\mathbf{u}}$ is included in the performance index J . The optimal static output feedback solution by Levine and Athans,¹⁹ which does not include the coupled weighting matrix, is generalized and obtained in the following. The gain matrix $\bar{\mathbf{G}}$ in equation (52) is obtained as

$$\bar{\mathbf{G}} = -\bar{\mathbf{R}}^{-1}(\bar{\mathbf{B}}'\bar{\mathbf{K}}\bar{\mathbf{L}}\bar{\mathbf{C}}' + \bar{\mathbf{S}}'\bar{\mathbf{L}}\bar{\mathbf{C}}')(\bar{\mathbf{C}}\bar{\mathbf{L}}\bar{\mathbf{C}}')^{-1} \quad (55)$$

where $\bar{\mathbf{K}}$ and $\bar{\mathbf{L}}$ satisfy the following non-linear equations:

$$\begin{aligned} \bar{\mathbf{M}}'\bar{\mathbf{K}} + \bar{\mathbf{K}}\bar{\mathbf{M}} + \bar{\mathbf{Q}} + \bar{\mathbf{S}}\bar{\mathbf{G}}\bar{\mathbf{C}} + \bar{\mathbf{C}}'\bar{\mathbf{G}}'\bar{\mathbf{S}}' + \bar{\mathbf{C}}'\bar{\mathbf{G}}'\bar{\mathbf{R}}\bar{\mathbf{G}}\bar{\mathbf{C}} &= 0 \\ \mathbf{I} + \bar{\mathbf{M}}\bar{\mathbf{L}} + \bar{\mathbf{L}}\bar{\mathbf{M}}' &= 0 \\ \bar{\mathbf{M}} &= \bar{\mathbf{A}} + \bar{\mathbf{B}}\bar{\mathbf{G}}\bar{\mathbf{C}} \end{aligned} \quad (56)$$

Note that equations (55) and (56) can be solved for $\bar{\mathbf{G}}$, $\bar{\mathbf{L}}$, $\bar{\mathbf{M}}$, $\bar{\mathbf{K}}$ iteratively. Once $\bar{\mathbf{G}}$ is obtained, the following procedures can be used to compute matrices \mathbf{N}_1 , \mathbf{N}_2 , L_{11} , L_{12} , L_{21} , L_{22} and D_2 of the compensator and P_1 , P_2 of the sliding surface: (i) $\bar{\mathbf{G}}$, H , N_1 and $(L_{11} - L_{12}P_2^{-1}P_1)$ can be determined from equation (52); (ii) with $\bar{\mathbf{G}}$ obtained in (i), N_2 can be determined from equation (54) by assigning non-singular P_2 , D_2 and any P_1 ; (iii) from equation (45) and H obtained above, L_{21} can be determined by assigning appropriate L_{22} ; (iv) since $(L_{11} - L_{12}P_2^{-1}P_1)$ is known, L_{11} can be determined by assigning appropriate L_{12} . L_{12} and L_{22} are chosen to guarantee the stability of the open-loop compensator equation. From a conservative point of view, a stable open-loop compensator equation is preferable in case the control force is saturated due to the limitation of the actuator capacity.¹²

ACKNOWLEDGEMENT

This paper is supported by the National Science Foundation through Grant No. CMS-96-25616.

REFERENCES

1. V. I. Utkin, *Sliding Modes in Control Optimization*, Springer, Berlin, 1992.
2. F. Zhou and D. G. Fisher, 'Continuous sliding mode control', *Int. J. Control* **55**(2), 313–327 (1992).
3. J. N. Yang, J. C. Wu and A. K. Agrawal, 'Sliding mode control for seismic-excited linear and nonlinear structures', *Technical Report NCEER-94-0017*, National Center for Earthquake Engineering Research, SUNY Buffalo, NY, 1994.
4. J. N. Yang, J. C. Wu and A. K. Agrawal, 'Sliding mode control of nonlinear and hysteretic structures', *ASCE J. Engng. Mech.* **121**(12), 1330–1339 (1995).
5. J. N. Yang, J. C. Wu and A. K. Agrawal, 'Sliding mode control of seismically excited linear structures', *ASCE J. Engng. Mech.* **121**(12), 1386–1390 (1995).
6. M. P. Singh, E. Matheu and L. E. Suarez, 'Active and semi-active control of structures under seismic Excitation', *Earthquake Engng. Struct. Dyn.* **26**(2), 193–213 (1997).
7. J. N. Yang, J. C. Wu, A. M. Reinhorn and M. Riley, 'Control of sliding-isolated buildings using sliding mode control', *ASCE J. Struct. Engng.* **122**(2), 83–91 (1996).
8. J. N. Yang, K. Kawashima and S. Unjoh, 'Hybrid control of seismic-excited bridge structures', *Earthquake Engng. Struct. Dyn.* **24**(11), 1437–1451 (1995).
9. J. N. Yang, J. C. Wu and Z. Li, 'Control of seismic-excited buildings using active variable stiffness systems', *J. Engng. Struct.* **18**(8), 589–596 (1996).
10. J. N. Yang, J. C. Wu, A. M. Reinhorn, M. Riley, W. E. Schmitendorf and F. Jabbari, 'Experimental verification of H_∞ and sliding mode control for seismic-excited buildings', *ASCE J. Struct. Engng.* **122**(1), 69–75 (1996).
11. S. V. Yallapragada and B. S. Heck, 'Optimal control design for variable structure systems with fixed order compensators', *Proc. American Control Conf.*, Vol. 1, 1992, pp. 876–880.
12. J. N. Yang, A. K. Agrawal and J. C. Wu, 'Sliding mode control of structures subjected to seismic loads', *Proc. 1st World Conf. on Structural Control*, Vol. 1, USC Publication, Los Angeles, 1994, pp. WA1-13 to WA1-22.
13. J. N. Yang, J. C. Wu, A. K. Agrawal and S. Y. Hsu, 'Reduced-order sliding mode control with compensators for seismic response control', *Proc. 11th World Conf. on Earthquake Engng.*, Acapulco, Mexico, Paper No. 273, 1996.
14. B. F. Spencer Jr, S. J. Dyke and H. S. Deoskar, 'Benchmark problems in structural control: Part I—Active mass driver system', *Earthquake Engng. Struct. Dyn.* **27**, 1127–1139 (1998).
15. B. F. Spencer Jr, S. J. Dyke and H. S. Deoskar, 'Benchmark problems in structural control: Part II—Active tendon system', *Earthquake Engng. Struct. Dyn.* **27**, 1141–1147 (1998).
16. J. N. Yang, J. C. Wu, A. K. Agrawal and S. Y. Hsu, 'Sliding mode control with compensators for wind and seismic response control', *J. Earthquake Engng. Struct. Dyn.* **26**, 1137–1156 (1997).
17. J. C. Doyle and G. Stein, 'Multivariable feedback design: concepts for a classical/modern synthesis', *IEEE Trans. Automat. Control* **AC-26**(1), 4–16 (1981).
18. E. J. Davison, 'A method for simplifying linear dynamic systems', *IEEE Trans. Automat. Control* **AC-11**(1), 93–101 (1966).
19. W. S. Levine and M. Athans, 'On the determination of the optimal constant output feedback gains for linear multivariable systems', *IEEE Trans. Automat. Control* **AC-15**(1), 44–48 (1970).